The International Journal of Cardiovascular Imaging (2019) 35:185–193
https://doi.org/10.1007/s10554-018-1432-z

ORIGINAL PAPER

Computationally simulated fractional flow reserve from coronary computed tomography angiography based on fractional myocardial mass

Huan Han[1] · Yong Gyun Bae[1] · Seung Tae Hwang[1] · Hyung-Yoon Kim[2] · Il Park[3] · Sung-Mok Kim[4] · Yeonhyeon Choe[4] · Young-June Moon[1] · Jin-Ho Choi[5]

Received: 6 June 2018 / Accepted: 1 August 2018 / Published online: 20 August 2018

Abstract

Computed tomography angiography (CCTA)-based calculations of fractional flow reserve (FFR) can improve the diagnostic performance of CCTA for physiologically significant stenosis but the computational resource requirements are high. This study aimed at establishing a simple and efficient algorithm for computing simulated FFR (S-FFR). A total of 107 patients who underwent CCTA and invasive FFR measurements were enrolled in the study. S-FFR was calculated using 145 evaluable coronary arteries with off-the-shelf softwares. FFR ≤ 0.80 was a reference threshold for diagnostic performance of diameter stenosis (DS) ≥ 50%, DS ≥ 70%, or S-FFR ≤ 0.80. FFR ≤ 0.80 was identified in 78 vessels (54%). In per-vessel analysis, S-FFR showed good correlation (r = 0.83) and agreement (mean difference = 0.02 ± 0.08) with FFR. The sensitivity, specificity, positive predictive value, negative predictive value, and accuracy of S-FFR ≤ 0.80 for FFR ≤ 0.80 were 84%, 92%, 92%, 83%, and 88%, respectively. S-FFR ≤ 0.80 showed much higher predictive performance for FFR ≤ 0.80 compared with DS ≥ 50% or DS ≥ 70% (c-statistics = 0.92 vs. 0.58 or 0.65, p < 0.001, all). The classification agreement between FFR and S-FFR was > 80% when the average of FFR and S-FFR was < 0.76 or > 0.86. Per-patient analysis showed consistent results. In this study, a simple and computationally efficient simulated FFR (S-FFR) algorithm is designed and tested using non-proprietary off-the-shelf software. This algorithm may expand the accessibility of clinical applications for non-invasive coronary physiology study.

Keywords Coronary circulation · Computational coronary physiology · Computed tomography

Abbreviations

3D	3-Dimensional
CAG	Coronary angiography
CFD	Computational flow dynamics
CCTA	Coronary computed tomography angiography
DS	Diameter stenosis
FFR	Fractional flow reserve
IDI	Integrated discrimination improvement
NPV	Negative predictive value
NRI	Net reclassification improvement
PPV	Positive predictive value
ROC	Receive-operating characteristics

Drs. Jin-Ho Choi and Young-June Moon are co-corresponding authors.

✉ Young-June Moon
yjmoon@korea.ac.kr

✉ Jin-Ho Choi
jhchoimd@gmail.com

[1] Computational Fluid Dynamics and Acoustics Laboratory, School of Mechanical Engineering, Korea University, Anamdong 5Ga, Seongbuk-gu, Seoul 136-713, Republic of Korea

[2] Department of Medicine, Chonnam National University Medical School, Gwangju, Republic of Korea

[3] Department of Medicine, Samsung Medical Center, Sungkyunkwan University School of Medicine, Seoul, Republic of Korea

[4] Department of Radiology, Samsung Medical Center, Sungkyunkwan University School of Medicine, Seoul, Republic of Korea

[5] Department of Emergency Medicine, Samsung Medical Center, Sungkyunkwan University School of Medicine, 81 Ilwon-ro, Gangnam-gu, Seoul 135-710, Republic of Korea

Introduction

An important criterion for the diagnosis of coronary artery disease is the detection of significant coronary artery stenosis that induces myocardial ischemia. Assessment of stenosis using invasive coronary angiography is a critical step in deciding on the treatment strategy. However, anatomical stenosis of coronary artery is a poor predictor for physiological severity of stenosis [1]. Coronary computed tomography angiography (CCTA) enables highly sensitive non-invasive visualization of coronary artery stenosis. Hence physiology-guided revascularization is considered to be superior to anatomy-guided revascularization in terms of improved clinical outcome and saving medical cost [2, 3]. Determination of physiological severity of stenosis from CCTA might be useful in clinical decision-making and guide appropriate treatment strategy.

Fractional flow reserve (FFR) is a widely accepted gold standard of physiologically significant arterial stenosis. FFR measurement requires invasive coronary angiography and a dedicated intracoronary pressure wire system. Obtaining non-invasive computational FFR using computational fluid dynamics-based interpretations of coronary artery geometry has emerged as an attractive alternative new diagnostic technology, and the systems are available from several vendors [4–6]. However, expensive proprietary systems and high-performance computational resources are required for non-invasive computational FFR, which limits the penetration of this technology in clinical practice. We developed a simple and computationally efficient simulated FFR (S-FFR) algorithm that can be implemented with commercially available off-the-shelf software toolkits. S-FFR calculated from patient-specific CCTA data was tested against invasively acquired FFR values and angiographic diameter stenosis (DS) measurements.

Methods

Patients

We retrospectively enrolled a total of 107 consecutive CCTA cases followed by invasive coronary angiography (CAG) and FFR measurement within 8 weeks and without intervening cardiovascular event from September 2014 to May 2016. Patients with prior revascularization, myocardial infarction, or significant structural heart disease were not included. Samsung Medical Center institutional review board approved this study investigating anonymized image and physiological data and informed consent was waived.

CCTA and FFR acquisition

A second-generation dual-source CT scanner (SOMATOM Definition Flash, Siemens Medical) was used as described previously [7, 8]. Contrast intravenous infusion comprised 70 ml of iomeprol (350 mg I/ml, Bracco) followed by 40 ml of saline at a rate of 4 ml/s. Images were acquired in the prospective ECG-triggered high-pitch (pitch 3.2–3.4) helical mode and were reconstructed using 0.5 or 0.6 mm slices. Using the radiation-reduction technique (CARE-Dose4D; Siemens), the mean effective radiation dose was 3.6 mSv.

CAG procedure and FFR measurements were performed as previously described [7, 8]. FFR was measured using a pressure wire (PressureWire Certus, Abott, IL) under adenosine-induced maximal hyperemia. FFR values ≤ 0.80 were considered indicative of physiologically significant stenosis.

Coronary artery anatomy reconstruction

Three-dimensional (3D) models of coronary artery tree and left ventricular myocardium were reconstructed using a dedicated imaging workstation (iNtuition, Terarecon, CA) as previously described [7, 8]. All major epicardial coronary arteries and branches ≥ 1.0 mm in diameter were traced from the ostium to distal end to build patient-specific geometrical mesh models. The amount of the left ventricular myocardium subtended by each major coronary artery was determined by fractional myocardial mass, which is vessel-specific myocardial mass calculated using the allometric scaling law and Huo and Kassab's stem-and-crown model [7–12]. Fractional myocardial mass was calculated by dividing the whole myocardial mass by the 4/3th power of the total arterial tree length as described in previous studies [7, 8].

Computational flow dynamics

The overall computational flow dynamics (CFD) workflow is shown in Fig. 1. In brief, Navier–Stokes equation was solved to compute the coronary blood flow mechanics within the geometrically reconstructed coronary artery tree. Proper boundary conditions were imposed on the finite volumetric mesh domain with realistic geometry. The blood flow rate through left or right coronary artery ostium was defined in terms of fractional myocardial mass of each artery and theoretically maximal hyperemic myocardial flow, which was sixfold increase of basal myocardial flow (5.4 ml/g/min) [13]. A steady inlet pressure of

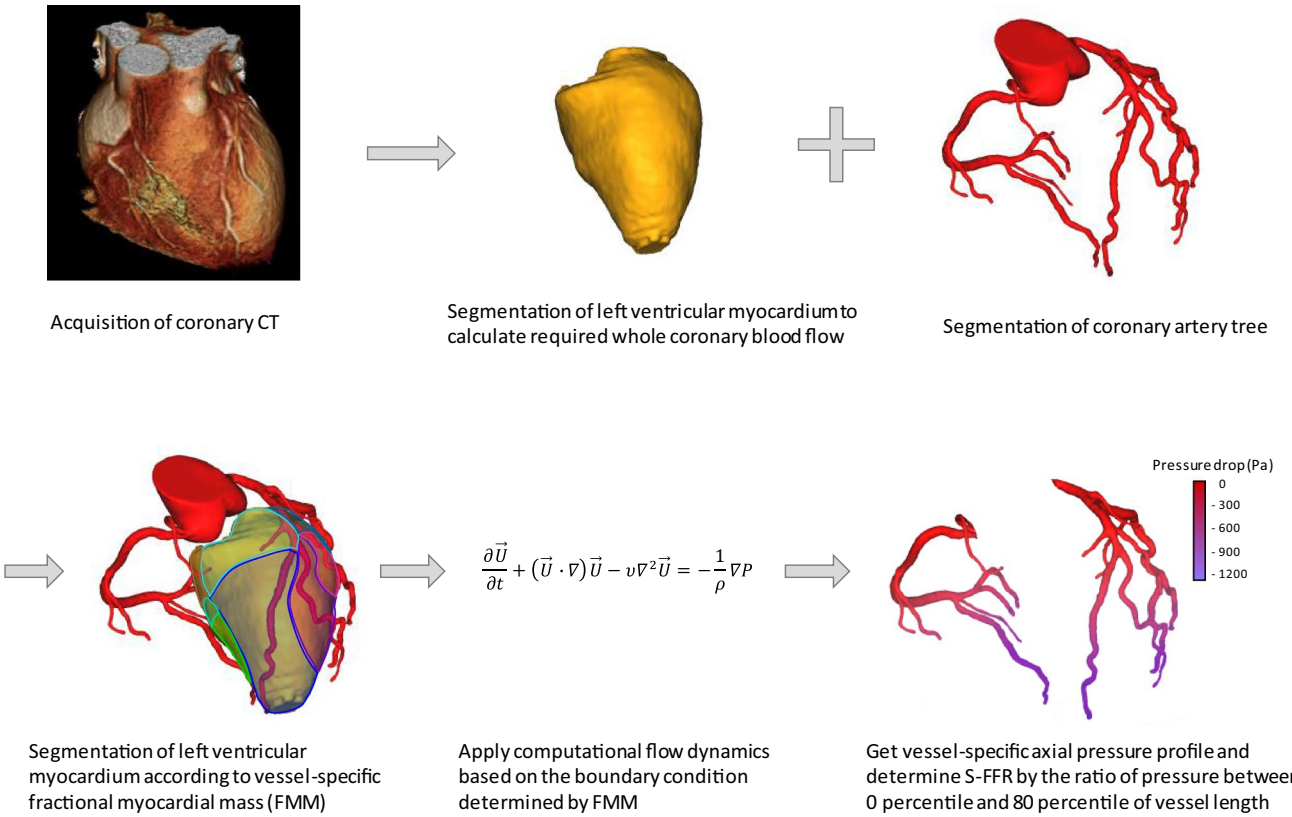

Fig. 1 Geometrical reconstruction of coronary artery anatomy and computational simulation of fractional flow reserve. The workflow of computationally simulated FFR (S-FFR) algorithm. Digitized 3-dimensional geometry of coronary artery tree and left ventricular myocardium is reconstructed from CCTA. The boundary condition is determined by fractional myocardial mass, a vessel-specific amount of myocardium. CFD is solved for the model with assumed continuous non-compressible Newtonian fluid flow. Numerical value of S-FFR is defined by the ratio of pressure drop between 0th and 80th percentiles of axial vessel length

100 mmHg was assumed. The exit boundary condition was determined as the split ratio of the mass flow at each bifurcation or trifurcation point according to the proportion of fractional myocardial mass subtended by each branch.

PointWise (PointWise, TX) generated a computational discrete grid from digitized 3D geometry of coronary arterial tree. Meshes at the branch junctions, stenotic segments, and near the wall were refined and concentrated with a high special resolution. A total of 11 prism layers were imposed on the flow with the initial thickness of 0.01 mm and growth rate of 1.1. The other parts were meshed with a user specified element, which we set to 0.3. Blood was assumed to be an incompressible Newtonian fluid with 1060 kg/m^3 density and 0.0045 pa s viscosity. Vessel walls were modeled as a non-slippery rigid solid. Mass conservation and momentum equations were solved within the 3D geometrical mesh comprising approximately 6 million grid cells. Simulations were calculated by CFD package STAR-CCM+ (Siemens PLM, TX) using the finite-element-method scheme. Grid independence test was done for model validation and showed that both coarse or fine grids exhibited a good consistency within a variation less than 3% after reaching a certain grid resolution. Simulation results were visualized by Matlab (MathWorks, MA) and Tecplot (Tecplot, WA). S-FFR was defined by the ratio of ostial arterial pressure to distal arterial pressure, which indicated pressure at the 0th and 80th percentiles of axial vessel length. Hemodynamically significant stenosis was defined as S-FFR $\leq$ 0.80. Representative cases are shown in Fig. 2.

Statistical analysis

Per-vessel or per-patient basis analysis was specified for each result. In case of multivessel measurement, vessel with the lowest FFR was used in per-patient analysis. Categorical variables are presented with frequencies and percentages. Continuous variables are presented with mean and standard deviation (SD) unless specified otherwise. FFR and QCA data were treated as continuous scale. DS $\geq$ 50%, DS $\geq$ 70%, FFR $\leq$ 0.80, and S-FFR $\leq$ 0.80 were treated as binary parameters for anatomically or functionally significant stenosis. Diagnostic sensitivity,

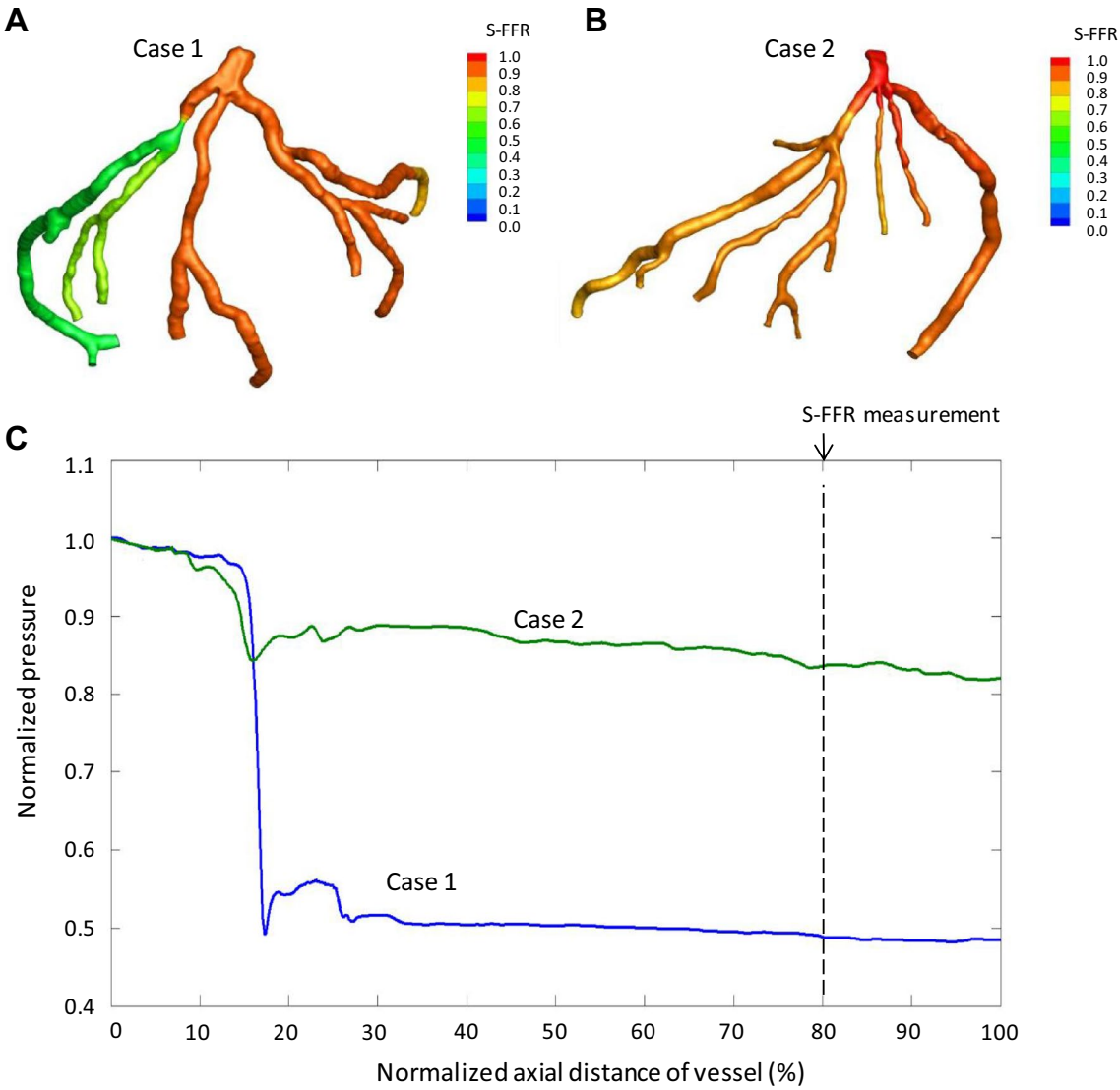

Fig. 2 Pressure profile of S-FFR along the vessel axial path. Representative cases of physiologically significant stenosis (**a**) and insignificant stenosis (**b**). Pressure profile from proximal to distal vessel (**c**)

specificity, positive predictive value (PPV), negative predictive value (NPV), and accuracy are presented with proportions and 95% confidence intervals. The conformity between S-FFR and FFR was tested by Spearman's rank test and Bland–Altman plot. Predictive performance of S-FFR or DS for FFR ≤ 0.80 was evaluated and compared in terms of receiver-operating characteristics (ROC) using DeLong's method, and reclassification analyses including net reclassification improvement (NRI) and integrated discrimination improvement (IDI). Per-range agreement was assessed by plotting the diagnostic accuracy against the average of FFR and S-FFR values using 10 equal sized groups [14]. Two-tailed $p < 0.05$ was considered statistically significant. R version 3.4 (R foundation) was used for statistical analysis.

Results

Patients and CCTA

The clinical characteristics of 107 patients are summarized in Table 1. The median interval between CCTA and invasive coronary angiography was 16 days. A total of 154 vessels were interrogated by FFR measurement. After excluding of 9 severely calcified vessels which were unsatisfactory for luminal reconstruction, 145 vessels (94.2%) including 94 left anterior descending artery, 21 left circumflex artery, and 30 right coronary artery were included in analysis. Diameter stenosis (DS) $\geq 50\%$ and $\geq 70\%$ were found in 121 (79%) and 37 vessels (24%), respectively. FFR ≤ 0.80 was found in 79 vessels (51%).

Table 1 Clinical characteristics

Number of patients	107
Age (year)	65 ± 10
Male gender	72.9 (78)
Diabetes	56.1 (60)
Hypertension	58.9 (63)
Smoking	44.9 (48)
Clinical diagnosis	
Stable angina	65.4 (70)
Unstable angina	18.7 (20)
Silent ischemia	15.9 (17)
Hemoglobin (mg/dl)	14.2 ± 1.3
Creatinine (mg/dl)	0.98 ± 0.46
Total cholesterol (mg/dl)	169 ± 38
LDL-cholesterol (mg/dl)	106 ± 35
HDL-cholesterol (mg/dl)	52 ± 11
Triglyceride (mg/dl)	112 ± 44

Shown as % (N) or median (interquartile range)

FFR versus S-FFR

S-FFR showed good correlation with FFR (Spearman's rank correlation = 0.828, p < 0.001, Fig. 3a). S-FFR slightly underestimated physiological stenosis. The mean and SD of FFR and S-FFR were 0.74 ± 0.15 and 0.77 ± 0.14, respectively. The mean difference between FFR and S-FFR was 0.02 ± 0.08 (Fig. 3b).

Diagnostic performance of S-FFR and CCTA for functionally significant stenosis

The discriminative performance of S-FFR ≤ 0.80 for FFR ≤ 0.80 was higher than CCTA DS ≥ 50% by (c-statistics = 0.92 vs. 0.58, p < 0.001; Fig. 4a). The sensitivity, specificity, PPV, NPV, and accuracy of S-FFR ≤ 0.80 for FFR ≤ 0.80 were 84% (95% confidence interval = 74–91%), 91% (81–97%), 92% (83–97%), 82% (71–90%), and 87% (80–92%) (Fig. 4b). The discriminative performance of S-FFR ≤ 0.80 was also higher compared to CCTA DS ≥ 70% (c-statistics = 0.92 vs. 0.65, p < 0.001) (Fig. 4c, d). Per-patient analysis also showed consistent results (Fig. 4e–h).

S-FFR consistently improved on the reclassification of FFR ≤ 0.80 over CCTA DS ≥ 50% or CCTA DS ≥ 70% (categorical NRI = 0.44–0.76, continuous NRI = 1.43–1.50, IDI = 0.43–0.52, p < 0.001, all) (Table 2).

Classification agreement of FFR and S-FFR

Both S-FFR and FFR showed unimodal distributions when presented in histograms (Fig. 5a, b). The per-range classification agreement between FFR and S-FFR was > 80% in most ranges of averages between S-FFR and FFR. The gray zone in which classification agreement < 80% was the average between S-FFR and FFR = 0.76–0.86 (Fig. 5c).

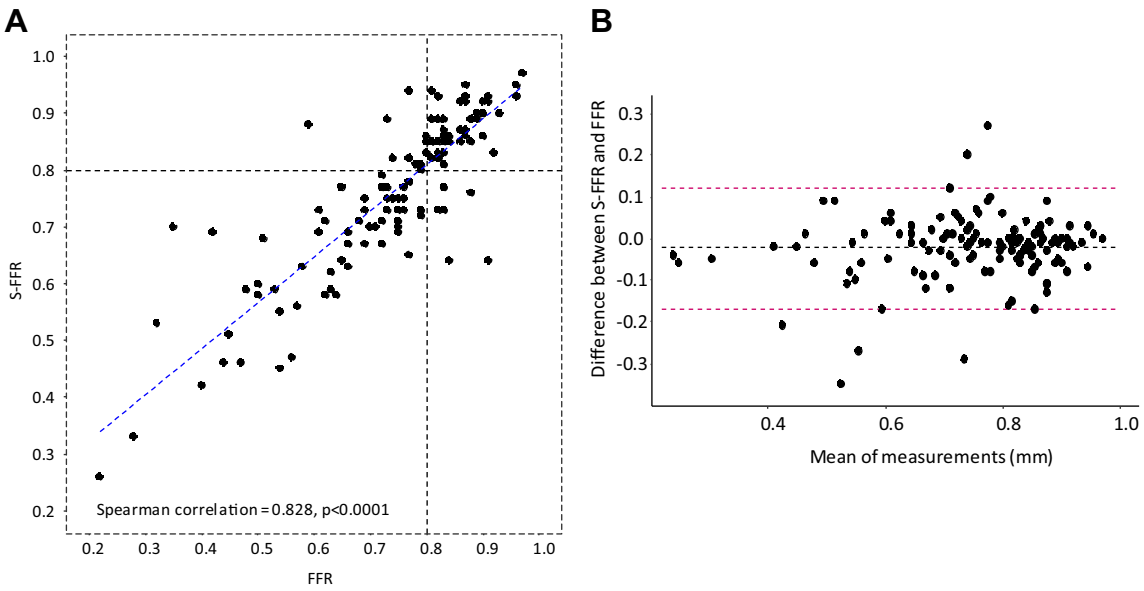

Fig. 3 Comparison of S-FFR with FFR. Per-vessel data is shown. **a** FFR and S-FFR showed good correlation (Spearman rho = 0.828). The mean FFR and S-FFR were 0.74 ± 0.15 and 0.77 ± 0.14, respectively. **b** The mean difference between FFR and S-FFR was 0.02 ± 0.08 in the Bland–Altman plot

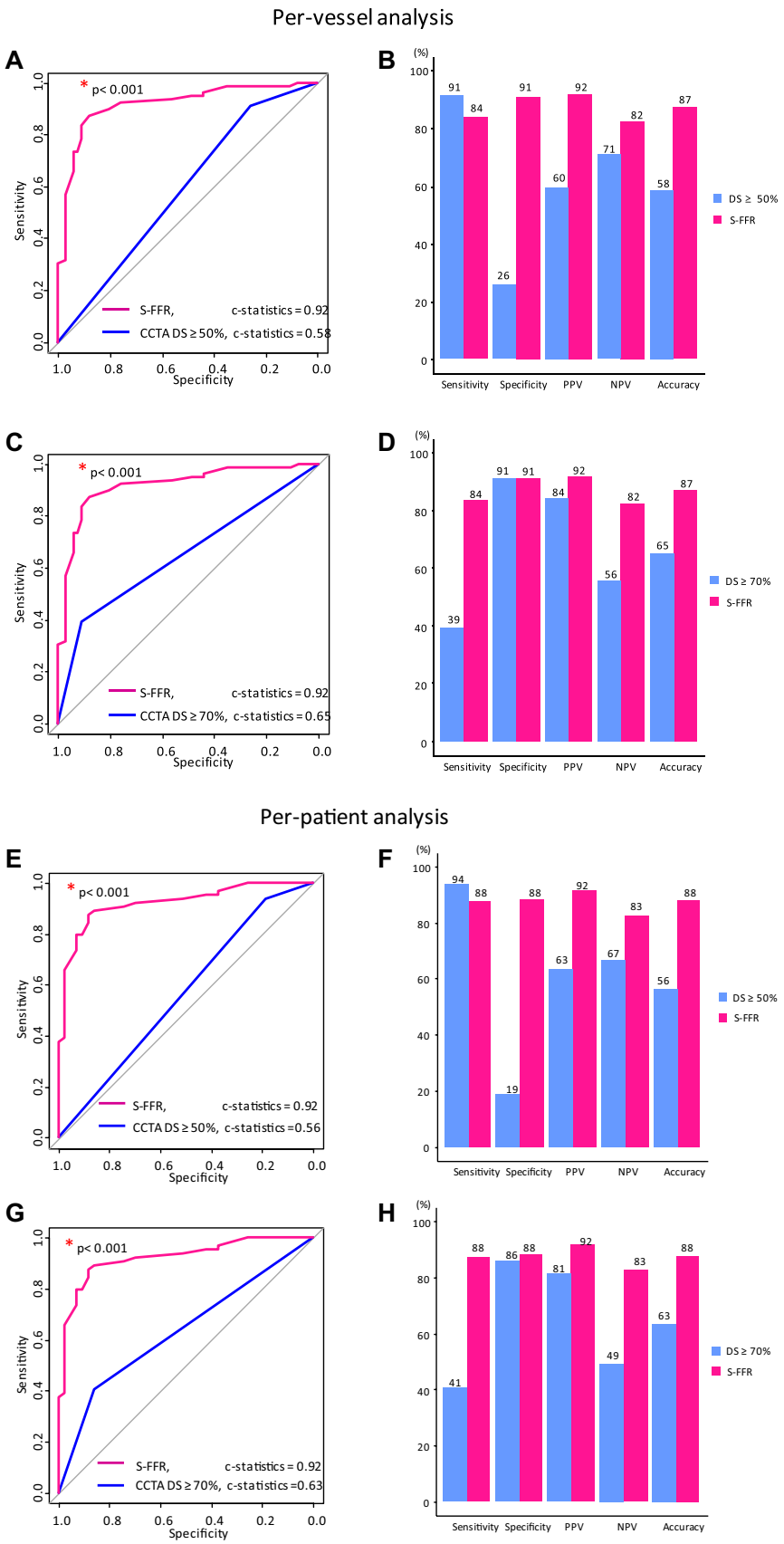

Fig. 4 Comparison of S-FFR and CCTA for diagnosis of physiologically significant stenosis defined by FFR ≤ 0.80. Per-vessel analyses (145 vessels) and per-patient analyses (107 patients) are shown in panels **a**–**d** and **e**–**h**, respectively. Note panels **a, b, d, f** use CCTA DS ≥ 50% and panels **c, d, g, h** use CCTA DS ≥ 70% for comparison with S-FFR. Compared with CCTA DS ≥ 50% or ≥ 70%, S-FFR showed higher discriminative performance for physiologically significant stenosis defined by FFR ≤ 0.80 (c-statistics = 0.92 versus 0.58 or 0.65, p < 0.001, all) (**a, c**). Increased accuracy of S-FFR for FFR ≤ 0.80 was driven by improved specificity and positive predictive value (**b, d**). Per-patient analysis showed consistent results (**e**–**h**)

Table 2 Reclassification of the diameter stenosis by computationally simulated FFR

	NRI (categorical)	NRI (continuous)	IDI
Per-vessel analysis			
CCTA DS ≥ 50%	0.58 (0.41–0.74)	1.45 (1.23–1.68)	0.49 (0.41–0.58)
CCTA DS ≥ 70%	0.44 (0.29–0.60)	1.43 (1.21–1.66)	0.43 (0.34–0.52)
Per-patient analysis			
CCTA DS ≥ 50%	0.64 (0.45–0.82)	1.47 (1.21–1.73)	0.52 (0.43–0.63)
CCTA DS ≥ 70%	0.76 (0.63–0.88)	1.50 (1.25–1.75)	0.48 (0.38–0.58)

CCTA coronary CT angiography, *DS* diameter stenosis. $p < 0.001$, all

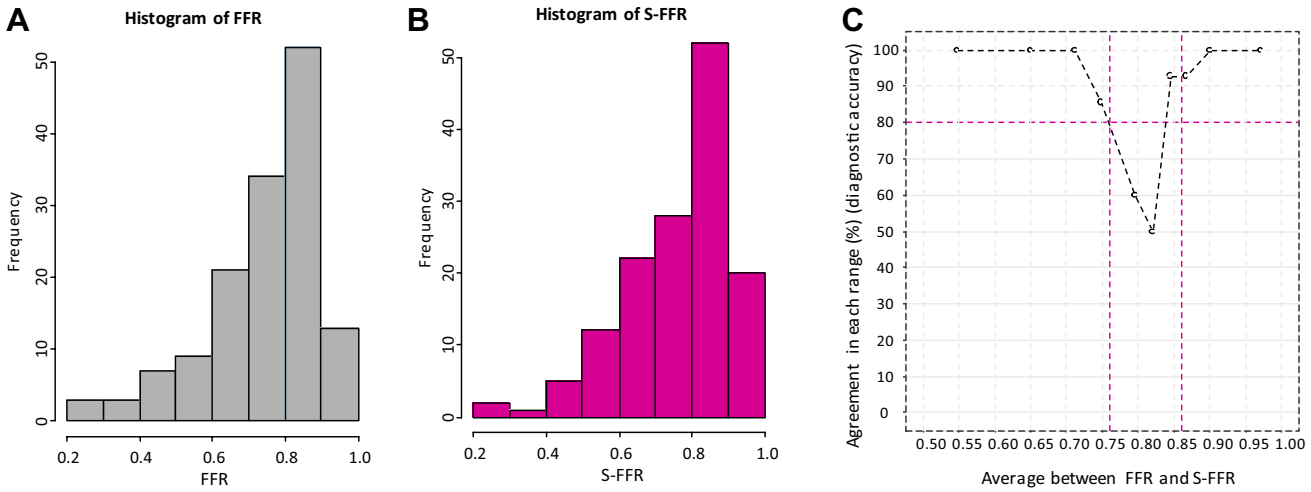

Fig. 5 Distribution and per-range agreement between S-FFR and FFR. **a, b** Histogram of FFR and S-FFR showed unimodal distribution. **c** Per-range classification agreement of S-FFR against FFR was > 80% when the average of FFR and S-FFR was < 0.76 or > 0.86

Discussion

We introduced a novel, simple, and efficient computationally simulated FFR algorithm based on boundary conditions defined by fractional myocardial mass. Importantly, the results were derived from conventional CT equipment without using any stress agents or pre-specified image acquisition conditions. All analyses were performed using commercially available off-the-shelf software. S-FFR may provide the basis of a vendor-independent computational FFR algorithm that could lower the threshold or investigator-initiated development of computationally simulated coronary physiology measurements.

S-FFR is different from the previously published proprietary computational FFR algorithms in the following respects. Unlike most proprietary algorithms on the basis of lumped element modeling which uses an analogy with an electric circuit to model coronary physiology using resistance, current, and voltage [6, 15–17], S-FFR is not based on the signal processing required for lumped element modeling but is based on the boundary conditions of blood flow determined by fractional myocardial mass. The assumed myocardial flow reserve is 6, which is higher than the value of 3 used in one proprietary computational FFR algorithm [18]. Both values are higher than coronary flow reserve of 2, which has been measured in numerous clinical studies [19–21]. S-FFR does not account for microvascular resistance. Despite these large differences, the accuracy of S-FFR (87%) was numerically not less accurate than current computational FFR algorithms (82% in pooled analysis) [5, 22].

The moderate diagnostic performance of computational FFR algorithms can be explained by the limited spatial or temporal resolution of CT images and the assumption of fixed boundary condition that in fact vary greatly between individuals [5, 22, 23]. Our results strongly suggest that the exclusion of uncertain parameters does not affect the efficacy of computational FFR algorithms. Interestingly, the gray zone of S-FFR against FFR in which classification agreement < 80% was 0.76–0.86, which is comparable to the gray zone of instantaneous wave-free ratio (iFR) against FFR, 0.78–0.88, and is numerically narrower than the gray zone of computational FFR of proprietary systems against FFR, 0.63–0.83 [5, 7, 14, 24]. If the efficacy of algorithms are comparable, the most simple and compact algorithm will

preferably minimize computational burden and lower the threshold for clinical application and study of computational FFR.

Limitations

This study investigated moderate number of cases enrolled in single center. Our model is not free from the inherent limitations on the application of CFD for coronary physiology simulations, such as accuracy of vessel reconstruction and patient-specific tuning of boundary conditions [25]. S-FFR does not take account of the patient-specific extent of maximal hyperemia, microvascular resistance, or left ventricular diastolic filling pressure. Like the other CCTA-based computational FFR algorithms, S-FFR is not applicable when accurate 3D luminal contours cannot be traced in severely calcified or poorly delineated vessels. Advanced CT scanner with finer spatial resolution and refined imaging software would be required for improving CCTA-based computational FFR algorithm. Vessels without stenosis or extremely stenotic vessels were not tested with invasive FFR measurement and were not included because such vessels do not need FFR measurement for clinical decision-making, although inclusion of such vessels would further increase the accuracy statistics for S-FFR. Although the algorithm of S-FFR is built from widely available toolkits and should be reproducible by the hands of trained technicians and engineers, further application of S-FFR in clinical settings would require appropriately powered validation with an independent multicenter study.

Impact of daily practice

We developed a simple and computationally efficient simulated fractional flow reserve (S-FFR) algorithm using non-proprietary off-the-shelf software. S-FFR showed good correlation and agreement with FFR. S-FFR ≤ 0.80 showed much higher predictive performance for FFR ≤ 0.80 compared with diameter stenosis. In wide range of the average of FFR and S-FFR (< 0.76 or > 0.86), the classification agreement between FFR and S-FFR was $> 80\%$. S-FFR may expand the accessibility of clinical applications for non-invasive coronary physiology study.

Acknowledgements We thank Seon A Jeong and So Hyeon Park for their excellent and devoted contributions.

Funding This study was funded by This study was supported by Korean Society of Circulation Grant (201301-01), Korean Society of Interventional Cardiology Grant [2014-1], Samsung Biomedical Research Institute Grant [GL1B33211], Samsung Medical Center Heart Vascular and Stroke Institute Clinical Research Project (OTC1601861), and National Research Foundation of Korea (2017R1A2B3010918).

Compliance with ethical standards

Conflict of interest The authors declare that they have no conflict of interest.

Ethical approval All procedures performed in studies involving human participants were in accordance with the ethical standards of the institutional and/or national research committee and with the 1964 Helsinki declaration and its later amendments or comparable ethical standards.

Informed consent Samsung Medical Center institutional review board approved this study investigating anonymized image and physiological data and informed consent was waived.

References

1. Ahn JM, Park DW, Shin ES et al (2017) Fractional flow reserve and cardiac events in coronary artery disease: data from a prospective IRIS-FFR registry (Interventional Cardiology Research Incooperation Society Fractional Flow Reserve). Circulation 135:2241–2251
2. De Bruyne B, Fearon WF, Pijls NH et al (2014) Fractional flow reserve-guided PCI for stable coronary artery disease. N Engl J Med 371:1208–1217
3. Johnson NP, Toth GG, Lai D et al (2014) Prognostic value of fractional flow reserve: linking physiologic severity to clinical outcomes. J Am Coll Cardiol 64:1641–1654
4. Min JK, Leipsic J, Pencina MJ et al (2012) Diagnostic accuracy of fractional flow reserve from anatomic CT angiography. JAMA 308:1237–1245
5. Cook CM, Petraco R, Shun-Shin MJ et al (2017) Diagnostic accuracy of computed tomography-derived fractional flow reserve: a systematic review. JAMA Cardiol 2:803–810
6. Trobs M, Achenbach S, Rother J et al (2016) Comparison of fractional flow reserve based on computational fluid dynamics modeling using coronary angiographic vessel morphology versus invasively measured fractional flow reserve. Am J Cardiol 117:29–35
7. Kim HY, Lim HS, Doh JH et al (2016) Physiological severity of coronary artery stenosis depends on the amount of myocardial mass subtended by the coronary artery. JACC Cardiovasc Interv 9:1548–1560
8. Kim HY, Doh JH, Lim HS et al (2017) Identification of coronary artery side branch supplying myocardial mass that may benefit from revascularization. JACC Cardiovasc Interv 10:571–581
9. West GB, Brown JH, Enquist BJ (1997) A general model for the origin of allometric scaling laws in biology. Science 276:122–126
10. Seiler C, Kirkeeide RL, Gould KL (1993) Measurement from arteriograms of regional myocardial bed size distal to any point in the coronary vascular tree for assessing anatomic area at risk. J Am Coll Cardiol 21:783–797
11. Huo Y, Kassab GS (2012) Intraspecific scaling laws of vascular trees. J R Soc Interface 9:190–200
12. Choy JS, Kassab GS (2008) Scaling of myocardial mass to flow and morphometry of coronary arteries. J Appl Physiol 104:1281–1286
13. Duncker DJ, Bache RJ (2008) Regulation of coronary blood flow during exercise. Physiol Rev 88:1009–1086
14. Petraco R, Escaned J, Sen S et al (2013) Classification performance of instantaneous wave-free ratio (iFR) and fractional flow reserve in a clinical population of intermediate coronary stenoses: results of the ADVISE registry. EuroIntervention 9:91–101

15. Koo BK, Erglis A, Doh JH et al (2011) Diagnosis of ischemia-causing coronary stenoses by noninvasive fractional flow reserve computed from coronary computed tomographic angiograms. Results from the prospective multicenter DISCOVER-FLOW (diagnosis of ischemia-causing stenoses obtained via noninvasive fractional flow reserve) study. J Am Coll Cardiol 58:1989–1997
16. Kruk M, Wardziak L, Mintz GS et al (2014) Accuracy of coronary computed tomography angiography vs intravascular ultrasound for evaluation of vessel area. J Cardiovasc Comput Tomogr 8:141–148
17. Tu S, Barbato E, Koszegi Z et al (2014) Fractional flow reserve calculation from 3-dimensional quantitative coronary angiography and TIMI frame count: a fast computer model to quantify the functional significance of moderately obstructed coronary arteries. JACC Cardiovasc Interv 7:768–777
18. Taylor CA, Fonte TA, Min JK (2013) Computational fluid dynamics applied to cardiac computed tomography for noninvasive quantification of fractional flow reserve: scientific basis. J Am Coll Cardiol 61:2233–2241
19. Cho SG, Park KS, Kim J et al (2017) Coronary flow reserve and relative flow reserve measured by N-13 ammonia PET for characterization of coronary artery disease. Ann Nucl Med 31:144–152
20. Johnson NP, Kirkeeide RL, Gould KL (2012) Is discordance of coronary flow reserve and fractional flow reserve due to methodology or clinically relevant coronary pathophysiology? JACC Cardiovasc Imaging 5:193–202
21. Hwang D, Jeon KH, Lee JM et al (2017) Diagnostic performance of resting and hyperemic invasive physiological indices to define myocardial ischemia: validation With 13N-ammonia positron emission tomography. JACC Cardiovasc Interv 10:751–760
22. Wu W, Pan DR, Foin N et al (2016) Noninvasive fractional flow reserve derived from coronary computed tomography angiography for identification of ischemic lesions: a systematic review and meta-analysis. Sci Rep 6:29409
23. Johnson NP, Kirkeeide RL, Gould KL (2013) Coronary anatomy to predict physiology: fundamental limits. Circ Cardiovasc Imaging 6:817–832
24. Gaur S, Taylor CA, Jensen JM et al (2016) FFR derived from coronary CT angiography in Nonculprit lesions of patients with recent STEMI. JACC Cardiovasc Imaging 10(4):424–433
25. Morris PD, Narracott A, von Tengg-Kobligk H et al (2016) Computational fluid dynamics modelling in cardiovascular medicine. Heart 102:18–28